Journal of Thermal Analysis and Calorimetry
https://doi.org/10.1007/s10973-019-09108-5

# Recovery of ammonia from wastewater through chemical precipitation

## Investigating the kinetic mechanism and reactions pathway of struvite decomposition

**Lavinia Bianchi[1] · Kerry Kirwan[1] · Luca Alibardi[2] · Marc Pidou[3] · Stuart R. Coles[1]**

Received: 17 May 2019 / Accepted: 25 November 2019


**Abstract**
Chemical precipitation is a consolidated technique applied in wastewater treatment to remove and recover phosphorous and ammonium that remain in the effluent after the anaerobic digestion treatment. The precipitate is magnesium ammonium phosphate hexahydrate ($MgNH_4PO_4{\cdot}6H_2O$), also known as struvite, and it is sold as a slow-release fertiliser. However, the value of struvite is quite low and has a limited market. Furthermore, it precipitates with heavy metals and other impurities that need to be removed to make the fertiliser commercially viable. This study looked at the thermal decomposition of struvite to recover added value products and recycle the magnesium for further precipitation. A kinetic study was carried out to understand the mechanism of decomposition and the formation of the different solid phases, which is fundamental for the design and optimisation of the technology. The thermogravimetric study confirmed that thermal decomposition is possible, but ammonia could not be completely released below 250 °C. The thermal analysis also led to the determination of the energy required for the decomposition, found to be 1.87 kJ $g^{-1}$, which also includes the evaporation of water and ammonia. The kinetic study through the isoconversional method showed the presence of two major reactions, and the model-fitting approach identified the diffusion model as the best fit for the first reaction. The activation energy of the first reaction found with this method was 0.24 kJ $g^{-1}$, comparable with the data obtained from the isoconversional method. The two-stage decomposition reactions were proposed, and the final calcination product was confirmed as magnesium pyrophosphate, which could be used in agriculture or dissolved in diluted mineral acids solution to separate the phosphate from the magnesium.

**Keywords** Ammonia recovery · Struvite precipitation · Struvite thermal decomposition · Kinetic mechanism · Wastewater treatment

## Introduction

The level of pollution of all water sources continues to rise in line with the increase in global population. High concentration of nutrients such as phosphorous and nitrogen compounds (e.g. nitrates) causes eutrophication, which affect the aquatic life. Thus, this pollution requires treatment; a higher level of contaminants translates into higher use of energy and chemicals for their removal. Increasingly, strict regulations on the pollution limits have helped to pose a serious question on whether it is environmentally friendly and particularly economically sound to only remove these contaminants. As a result, the recovery of resources that can be exploited as fertilisers (e.g. phosphorous and ammonia) has gained attention in the wastewater

**Electronic supplementary material** The online version of this article (https://doi.org/10.1007/s10973-019-09108-5) contains supplementary material, which is available to authorized users.

✉ Stuart R. Coles
stuart.coles@warwick.ac.uk

[1] WMG, International Manufacturing Centre, University of Warwick, Coventry CV4 7AL, UK

[2] Severn Trent Water Ltd, Severn Trent Centre, 2 St John's Street, Coventry CV1 2LZ, UK

[3] Cranfield Water Science Institute, Cranfield University, Cranfield MK43 0AL, UK

Published online: 11 December 2019

sector. It is an opportunity to implement circular economy models as opposed to linear economy models which have dominated the twentieth century [1]. A circular economy model focuses on closing the loop and has the objective of reusing and recycling materials in order to reduce the environmental impact of the manufacturing of products, whilst in a linear model raw materials are used to produce a product which is discarded at the end of life [2]. Phosphorous is considered a limited resource on Earth [3]. Ammonia is one of the nitrogen-based compounds that can be found in wastewater and sludge. It must be removed because it is toxic and harmful to the environment, but it is also a valuable resource used in industry to produce nitrogen fertilisers; as such, its production has been rising constantly in the past decades, exceeding 140 million tonnes in 2016 [4]. Ammonia is obtained from the industrial fixation of nitrogen, through the Haber–Bosch process [5]. This process is typically powered by coal or methane; it is very energy intensive and accounts for more than 50% of the total world hydrogen consumption, which corresponds to 3.6 M tonnes [6, 7].

Most current wastewater treatment techniques concerned with nitrogen focus only on removal. Chemical precipitation is one of the few that recovers both phosphorous and ammonium in the form of magnesium ammonium phosphate hexahydrate (commonly known as struvite), which has applications as a slow-release fertiliser. The precipitation technique is used also in different waste streams, such as manure or pig slurry [8, 9], and has been introduced to overcome issues related to the spontaneous formation of struvite in pipelines after the anaerobic digestion treatment, where the effluent is rich in phosphorous and ammonium. These deposits cause blockages and inefficiencies that lead to additional maintenance operations and added costs [10]. Struvite is formed by the following reaction:

$$Mg^{2+}_{(aq)} + PO^{3-}_{4\,(aq)} + NH^{+}_{4\,(aq)} + 6H_2O_{(l)} \rightarrow MgNH_4PO_4 \cdot 6H_2O_{(s)} \quad (1)$$

The spontaneous formation of struvite is due to its low solubility product ($3.89 \times 10^{-10}$ at 25 °C in wastewater and $4.330 \times 10^{-14}$ at 25 °C in aqueous solution) [11, 12]. Magnesium is the limiting reagent since its concentration is typically lower when compared to the ammonium and phosphate ions. Therefore, a magnesium source (magnesium chloride, $MgCl_2$, or magnesium oxide, MgO) has to be added to the system, increasing the cost of the technology.

In recent years, researchers have started focusing on the possibility of decomposing struvite and recycling the magnesium source. As a result, research studies have shown that struvite can be thermally decomposed, releasing ammonia and water [13–15]. Through direct calcination, struvite loses water molecules and ammonia that evaporate from the solid, resulting in a mass loss of over 50%. However, the mechanism of decomposition is not yet clear. Sugiyama et al. [16] performed solid-state NMR and XRD at different temperatures and confirmed that the calcination of struvite involves the formation of $MgHPO_4$, which is then transformed into $Mg_2P_2O_7$. An amorphous compound was obtained at temperatures above 200 °C. This was contradicted by Bhuiyan et al. [14], who affirmed that the substance becomes amorphous as soon as the water molecules are evaporated; they also suggested $MgHPO_4$ as the final calcination product, corresponding to 51% mass loss. However, even though Sugiyama et al. indicated the composition of the intermediate compounds, no reaction mechanism was proposed. Many studies have confirmed that the decomposition is influenced by the heating rate [13, 14]. According to Frost et al. [13], with a heating rate of 2 °C $min^{-1}$ the decomposition started at 85 °C, but using 1 °C $min^{-1}$ the mass degradation started at circa 40 °C. In this study, it was concluded that at 1 °C $min^{-1}$ ammonia is lost before the water evaporates. Nonetheless, this was demonstrated by analysing the gases with mass spectrometry and was not proven by any elemental or quantitative analysis. In this respect, Bhuiyan reported that ammonia and water were lost simultaneously in one single stage, with the mass loss occurring faster at slower heating rates [14]. This was suggested by analysing the derivative curves of the thermogravimetric analysis. They also proposed a mechanism of the various phases related to struvite and heating through considerations of the XRD spectra in different phases of the decomposition. So far, the mechanism of decomposition of struvite and the possibility to obtain valuable products from it have not been clearly understood. As a result, this study has focused on struvite decomposition in the solid state and performed a kinetic analysis to investigate the mechanisms of the reactions involved.

## Materials and method

### General considerations

Commercial struvite (magnesium ammonium phosphate hexahydrate 98%) was sourced from VWR International Ltd, referred to as “struvite A”. Samples of struvite produced during the wastewater treatment process were provided by Severn Trent Water Ltd., referred to as “struvite B”. The samples were stored in sealed containers in a dry and cool place. All chemicals were used as received without any further purification.

### Elemental analysis

The samples were analysed using a CE 440 Elemental Analyser. These tests were used to determine the content of nitrogen in struvite after different stages of degradation. Struvite A and struvite B were also analysed by ICP-OES technique, using PE Optima 5300 Dual View ICP-OES Analyser. The samples were tested for the following elements, which include heavy metals whose limits must comply with EU regulations: As, Ca, Cd, Cr, Cu, Hg, Mg, Ni, P, Pb, Zn. The instrument measured to an accuracy of 0.1 ppm.

### Attenuated total reflection Fourier transform infrared (ATR-FTIR)

Fourier transform infrared spectrometry was performed at room temperature in the wave number range of 500–4000 $cm^{-1}$, using the attenuated total reflection method (ATR-FTIR; Cary Tensor 27). The samples, all in the form of a powder, were placed on the detecting crystal, and then, pressure was applied. The resulting spectrum was a mean of 24 scans with a resolution of 4 $cm^{-1}$. In few cases, the instrument was used in the transmittance mode, in which the spectra appear with an intensity from 0 to 100%.

### Thermogravimetric analysis (TGA)

Thermogravimetric analysis (TGA) was used to study the degradation of struvite A and struvite B. Three samples were tested for each test condition using Mettler Toledo TGA 1 STAR$^e$ System. Four different heating rates were applied (20 °C $min^{-1}$, 10 °C $min^{-1}$, 5 °C $min^{-1}$ and 0.5 °C $min^{-1}$) under nitrogen atmosphere (flow rate 50 mL $min^{-1}$), from 25 to 500 °C, using 70-µL alumina crucibles. Further tests were conducted in isothermal conditions, using the same crucibles under a nitrogen atmosphere. Each method was set up to keep the sample at a certain temperature for 5 h. The samples all weighed between 9 and 11 mg, and the mass loss was normalised afterwards.

### Differential scanning calorimetry (DSC)

The energy required to achieve complete degradation of struvite was calculated using the data gathered from differential scanning calorimetry analysis. The instrument used was a Mettler Toledo DSC 1 STAR$^e$ System and was programmed with different methods using $N_2$ flow of 11 mL $min^{-1}$ and 40-µL aluminium crucibles (as the reference pan). The pans were sealed and pierced in the centre, so that the volatiles could be released. The DSC measured the energy flow with respect to temperature in W $g^{-1}$.

## Results and discussion

Thermal and characterisation analyses were carried out on struvite A and struvite B to investigate their transformation during heating. A kinetic analysis was used to understand the decomposition mechanism.

### Material characterisation

Figure 1 (left) depicts the FTIR analysis of struvite A and struvite B. The spectra did not reveal any significant difference between struvite A and struvite B. In fact, the FTIR spectrometer detected two similar patterns that show the same important peaks that characterise struvite, as reported elsewhere [17, 18]. Two bands at 1431 and 1591 $cm^{-1}$ wavenumber can be observed, which corresponds to the H–N–H bond of ammonium [13]. The P–O band is present at 980 $cm^{-1}$ wavenumber. The 1591 $cm^{-1}$ band is attributed to the water bending mode. The band at 2359 $cm^{-1}$

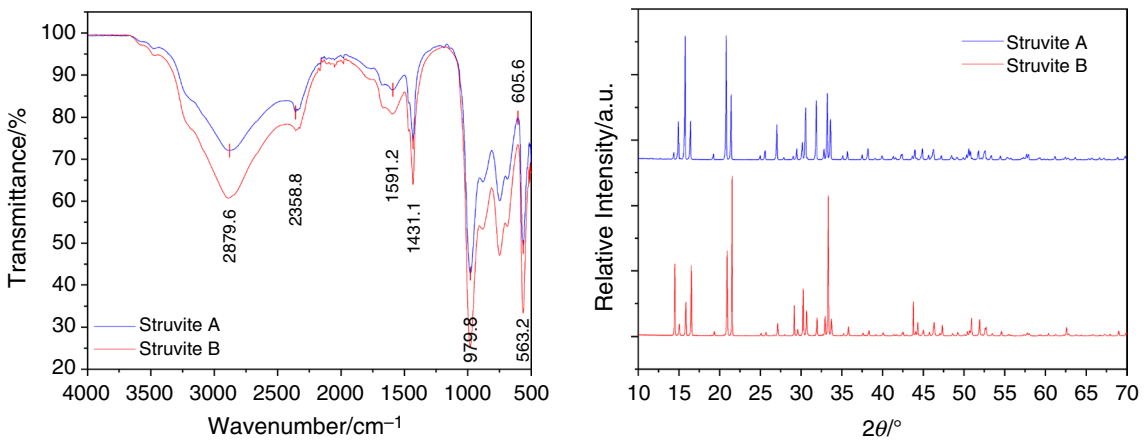


**Fig. 1** FTIR (left) from 4000 to 500 $cm^{-1}$ in transmittance mode and XRD (right) of struvite A and struvite B

wavenumber is associated with the water-related hydrogen bonding [19].

This remarkable similarity indicates that the impurities present in the struvite B did not affect the chemical structure of the sample. Moreover, the identical mineral phases of the two samples are confirmed by the XRD spectra (Fig. 1, right). Therefore, the materials, despite different sources, have the same chemical structure. However, SEM analysis revealed a difference in the morphology of the samples. Figure 2 shows the materials that for the test have been magnified 500 times. The image on the left regards the sample purchased by VWR, which presents a well-defined structure, with crystals of around 100 µm width. On the contrary, struvite B shown on the right has grains of various sizes, from 10 to more than 100 µm, and the crystals cannot be identified.

This might be due to an uncontrolled precipitation reaction (e.g. lack of pH control), which caused the formation of grains of irregular shape and size, whereas struvite A has well-defined crystals because the synthesis was regulated to obtain certain product specifications. In the literature, Le Corre et al. [20] reported how calcium impurities affected the precipitation. They varied the Ca:Mg ratio and saw how this had an influence on the crystal growth rate. The image of uncontrolled precipitation of struvite B is similar to other SEM analyses of struvite precipitation from wastewater reported elsewhere [21–23].

When comparing ICP results for magnesium and phosphorous with the theoretical values of struvite, it can be noticed how struvite B has a higher content of magnesium, 10.57% against 9.90% (Table 1). This can be attributed to a fraction of unreacted magnesium chloride present in the sample, which could also be related to uncontrolled precipitation. In fact, the table also shows how the values of commercial struvite Crystal Green® synthesised by the Ostara Technology are almost equal to the theoretical concentrations [24]. It can also be noted how the purchased struvite A presents higher magnesium content, coupled with almost 5% higher phosphorous content.

**Table 1** ICP-OES on struvite B, Mg and P concentrations expressed in % wt/wt

| Element | Unit | Struvite (theoretical values) | Struvite A | Struvite B | Commercial struvite (crystal green®), [24] |
|---|---|---|---|---|---|
| Mg | % | 9.90 | 11.34 | 10.57 | 10.00 |
| P | % | 12.60 | 17.42 | 12.41 | 12.60 |

The ICP-OES analysis also revealed the presence of impurities. Struvite A and struvite B were tested for several elements, including arsenic, cadmium, chromium, lead, nickel and mercury, which must be within the limits set by EU regulations. Table 2 compares the values with the current EU fertiliser regulation, the EC 2003/2003 [25]. The value of cadmium was converted from ppm to mg $kg^{-1}$ of $P_2O_5$, as this is how it is referred to in the regulation. The conversion was obtained by knowing the content of P in struvite and applying the conversion factor which is stated in the regulation ($P/P_2O_5 = 0.436$) [25]. Calcium resulted as the most abundant impurity with 5303 ppm, which may confirm it as the reason for which struvite B crystal morphology is so different from struvite A. Table 2 highlights that struvite A is highly pure, since the concentration of most metals is below 0.01 ppm. Calcium is the metal found with the highest concentration, which corresponds to 1.83 ppm.

Most of the contaminants that are present in struvite B are within the EU limits. However, the two elements that exceeded the maximum concentration were chromium and mercury. In addition to that, cadmium was just below the threshold of 60 mg $kg^{-1}$ $P_2O_5$. These metals are highly hazardous and represent a threat for soil contamination. Thus, these results show a limitation for the use of struvite B as a fertiliser, unless the recovered product is treated to reduce the content of these heavy metals.

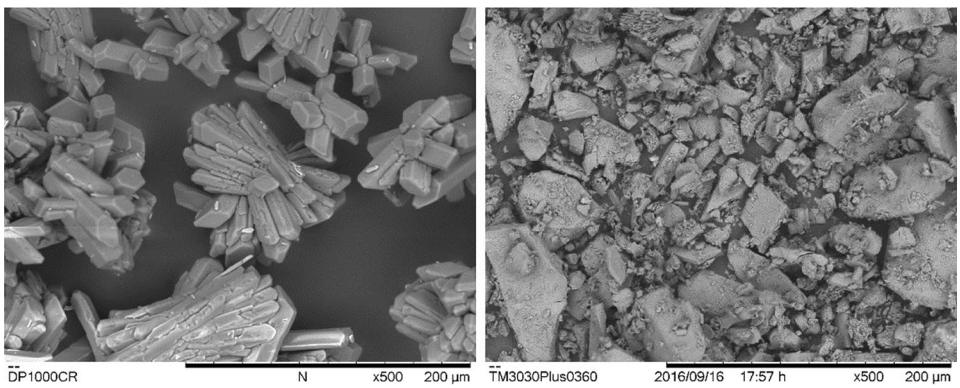


**Fig. 2** SEM images of struvite A (left) and struvite B (right)

**Table 2** ICP-OES on struvite B, metal concentrations expressed in ppm (* Cd concentration has been converted to mg $kg^{-1}$ $P_2O_5$ to compare it with Crystal Green and EU regulations)

| Element | Unit | Struvite A | Struvite B | EU current fertiliser regulation, EC 2003/2003 |
|---|---|---|---|---|
| As | ppm | 0.0000 | 30 | 60 |
| Ca | ppm | 1.8300 | 5303 | N.A. |
| Cd | ppm wt/wt | 0.0000 | 15.8 (=55.5 mg $kg^{-1}$ $P_2O_{5*}$) | 60 mg $kg^{-1}$ $P_2O_5$ |
| Cr | ppm | 0.0005 | 11 | 2 |
| Cu | ppm | 0.0060 | 12 | N/A |
| Hg | ppm | 0.0019 | < 5 | 2 |
| Ni | ppm | 0.0678 | 24 | 120 |
| Pb | ppm | 0.0015 | 19 | 150 |
| Zn | ppm | 0.0568 | 28.2 | N/A |

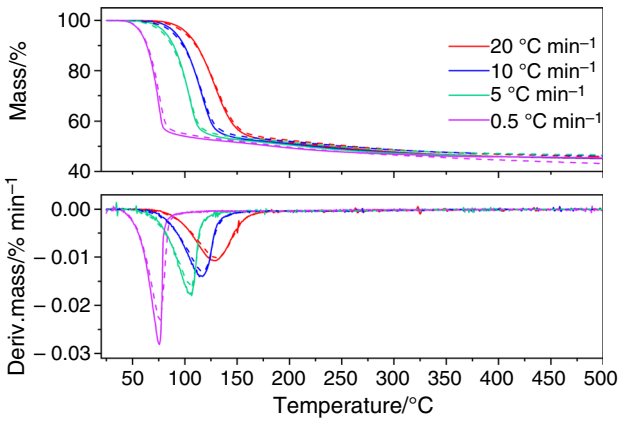


**Fig. 3** TG and DTG curves of struvite A (continuous line) and B (dash) at heating rates of 20, 10, 5, 0.5 °C $min^{-1}$; curves are the mean of three samples, average standard deviation below 0.3% apart from 0.5 °C $min^{-1}$ (< 1%)

## Heating rate influence on struvite degradation

Initial results highlighted the structured decomposition curves for each heating rate condition, with a significant mass loss up to 54.5%. As shown in the graphs of Fig. 3, the TG curve confirmed that the behaviour of struvite A and struvite B (continuous and dash lines, respectively) is similar. In fact, overall the curves are overlapped during the major mass loss.

However, the analysis resulted in a slight difference in the residual mass, with struvite B having an average of 46.280% from the initial sample, whereas struvite A had 45.281%. This discrepancy likely means that most contaminants are volatile. The difference of 1% could be attributed to the aforementioned excess of magnesium and non-volatile heavy metals. Overall, it could be confirmed that contaminants, at least in terms of mass loss rate, did not affect struvite degradation. This might suggest that, also from a kinetic point of view, there should not be a difference between struvite A and struvite B. From this analysis, it also emerged that the decomposition of both struvite A and struvite B is strongly dependent on the heating rate, as highlighted from the derivative curve (Fig. 3). Indeed, the calcination onset temperature decreased when the heating rate diminished, as previously reported in the literature [14, 26]. At 0.5 °C $min^{-1}$, struvite A started decomposing at 31.8 °C, and the temperature corresponding to the fastest decomposition was at 76.8 °C, whereas at 20 °C $min^{-1}$ the sample began to lose mass at 68.3 °C and reached its maximum rate only at 129 °C.

## Evidence of multi-stage degradation

Having considered the results of the first set of thermogravimetric tests, the second set of experiments was prepared with the objective of understanding the behaviour in the presence of isothermal conditions at different temperatures, in order to minimise the temperature and energy required to degrade struvite and remove the ammonia. In this regard, only struvite B was tested, having previously understood its remarkable similarity with struvite A. The temperatures were chosen based on the results of the previous TG test at the slowest heating rate (0.1 °C $min^{-1}$), in the range where the biggest mass loss occurred, and thus at 40, 50, 60 and 75 °C. The sample was kept in the furnace for 5 h for each condition.

The TG curves mainly indicate that no significant mass loss occurred below 60 °C in 5 h. Indeed, only 21.5% of the mass evaporated at 60 °C, whereas 42.2% is lost at 75 °C (Fig. 4). However, as mentioned above, the final calcination product presented 54.5% of mass loss; therefore, there was 12.3% of the compound that could not be released at that temperature. The samples heated at 60 and 75 °C were analysed with CHN to understand how much nitrogen was still present after the isothermal experiments. A decrease in the nitrogen content was observed: at 60 °C it was 4.27%, whereas at 75 °C it was 2.61%. This confirms that the part of

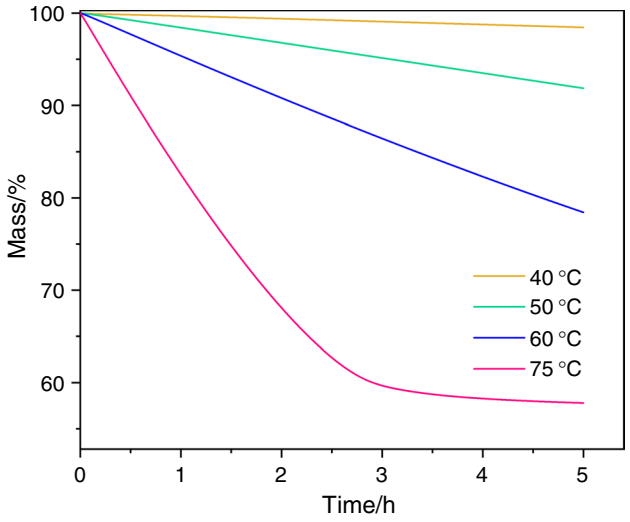


**Fig. 4** TG curve of isothermal tests on struvite B at temperatures of 40, 50, 60, 75 °C for 5 h

the ammonia evaporates together with water at temperatures below 100 °C, in accordance with Frost et al. [13]. The carbon content increased from 60 to 75 °C, and this indicates that the contaminants constituted by carbon are not volatile and remained in the calcination product. From this analysis, it emerged that from a process point of view the most important thermal conditions are the temperatures of 60 °C, 75 °C and above. Considering this, a multi-stage isothermal test was conducted in nitrogen atmosphere on struvite A with the following steps: 75 °C, 145 °C, 250 °C and 500 °C. The temperatures were chosen as intervals between 75 and 500 °C. For clarity, the DTG curve was smoothed and the white sections correspond to where the temperature is being increased, whereas the coloured sections indicate where isothermal conditions have been reached.

This experiment revealed that the degradation of struvite requires temperatures above 250 °C to reach completion (Fig. 5, left). In fact, the mass loss obtained from the test at 250 °C was no more than 53.9%, whereas from that temperature to 500 °C the sample lost another 2.50% of its mass. Maximum standard deviation was 1.05% for this test, and the variability may be due to higher moisture content in the samples. Thus, results are in line with the TG curves shown in Fig. 3. The FTIR spectra highlight how the ammonium peak ($\nu_4$ bending mode vibration at 1442 $cm^{-1}$) was still present at 250 °C (Fig. 5, right). Furthermore, from this graph it was possible to distinguish two different compounds: indeed, until 145 °C the spectra had similar peaks, maintaining the antisymmetric stretching $\nu_3$ of $HPO_4^{2-}$ and $PO_4^{3-}$ at 880, 1000 and 1062 $cm^{-1}$, whereas from 250 up to 500 °C the spectra revealed a different pattern in the fingerprint region. There is the formation of a peak at circa 750 $cm^{-1}$, which can be attributed to the bending vibrations of O–P–O, and a shift in the peaks present at 880, 1000 and 1062 $cm^{-1}$. This corresponds to the formation of new bonds and a change in the structure of the sample, which coincides with the transformation of $MgHPO_4$ into $Mg_2P_2O_7$, as suggested in the literature [14, 15].

## Characterisation of calcination products

The calcination product of struvite A obtained after heating up to 500 °C was analysed with CHN analysis, and the results showed that all the ammonia was evaporated during the thermal decomposition, leaving 0.15% wt/wt in the sample. In order to characterise the calcination product, some

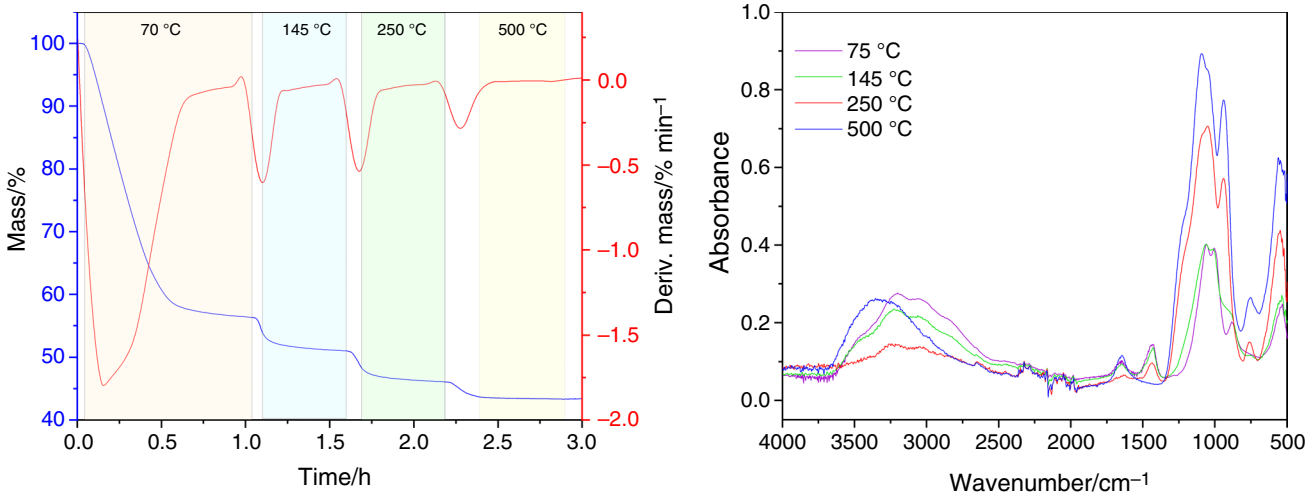


**Fig. 5** Multi-stage isothermal test on struvite A (left) and corresponding ATR-FTIR of the samples decomposed at the following temperatures: 75, 145, 250 and 500 °C (right)

chemicals of the ones attributed to the decomposition in the literature were tested with FTIR to compare their spectra with the one of the degraded samples. Magnesium pyrophosphate ($Mg_2P_2O_7$) has been reported more than once as a possible calcination product, but also magnesium phosphate [$Mg_3(PO_4)_2$] and magnesium hydrogen phosphate ($MgHPO_4$) have also been mentioned in several publications [13, 14, 16]. The findings from the FTIR shown in Fig. 6 are consistent with the findings previously reported, which mention the two broad peaks at 1105 and 929 $cm^{-1}$ as indication of the formation of $Mg_2P_2O_7$ [27, 28]. It must be taken into account also that the resolution of the instrument is 4 $cm^{-1}$, and therefore, these discrepancies are acceptable. Unfortunately, the loss of crystallinity upon heating did not allow the identification of the mineral phase. From this analysis, it can be concluded that the final calcination product is magnesium pyrophosphate.

## Energy required for the degradation

At this point, the differential scanning calorimetry technique was decisive to understand the energy required to evaporate completely the ammonia present in the compound. By knowing the heat capacity of struvite, it was possible to determine the heat required for the degradation. In this technique, the positive energy flow is associated with an exothermic reaction, whereas the negative peak indicates that the sample has absorbed energy. The resultant energy is not only the energy required for the degradation, but it also includes the energy absorbed by the sample in order to change the temperature. The energy flow can be expressed as:

$$\frac{dH}{dt} = C_p \frac{dT}{dt} + f(T,t)$$

Consequently, the enthalpy of the reaction can be calculated by the integral with respect to time of the energy flow. In the equation, $C_p$ is the sample heat capacity (measured in J $°C^{-1}$), which is defined as the specific heat (J $g^{-1}$ $°C^{-1}$) multiplied by the mass of the substance. The second part of the equation, $f(T,t)$, is related to the kinetic of the reaction and the phase transitions occurring in the material. In addition, when there is an isothermal condition, the only heat flow detected by the DSC machine must be due to a transformation in the sample. The experiment was programmed to heat the sample from 25 to 500 °C at 20 °C $min^{-1}$ in nitrogen atmosphere. The result of this test confirmed the presence of two major events taking place during the degradation. As represented in Fig. 7, the first peak is present during the greatest mass loss, whereas the second peak which was not detected in the derivative curve of the TG test is at circa 250 °C.

The curve was integrated in order to calculate the energy required for the degradation, and the value was found to be 1.87 kJ $g^{-1}$ at 10 °C $min^{-1}$ (1.371 kJ $g^{-1}$ for the first peak, 0.497 kJ $g^{-1}$). It is important to note that this energy value includes also the latent heat of vaporisation of both ammonia and water, which is reasonably embedded in the first peak and was calculated to be, respectively, 0.029 and 0.970 kJ $g^{-1}$. Therefore, the activation energy is obtained by detracting these values from the energy found for the first peak and is 0.37 kJ $g^{-1}$. Further information can be found in Online Resource 1.

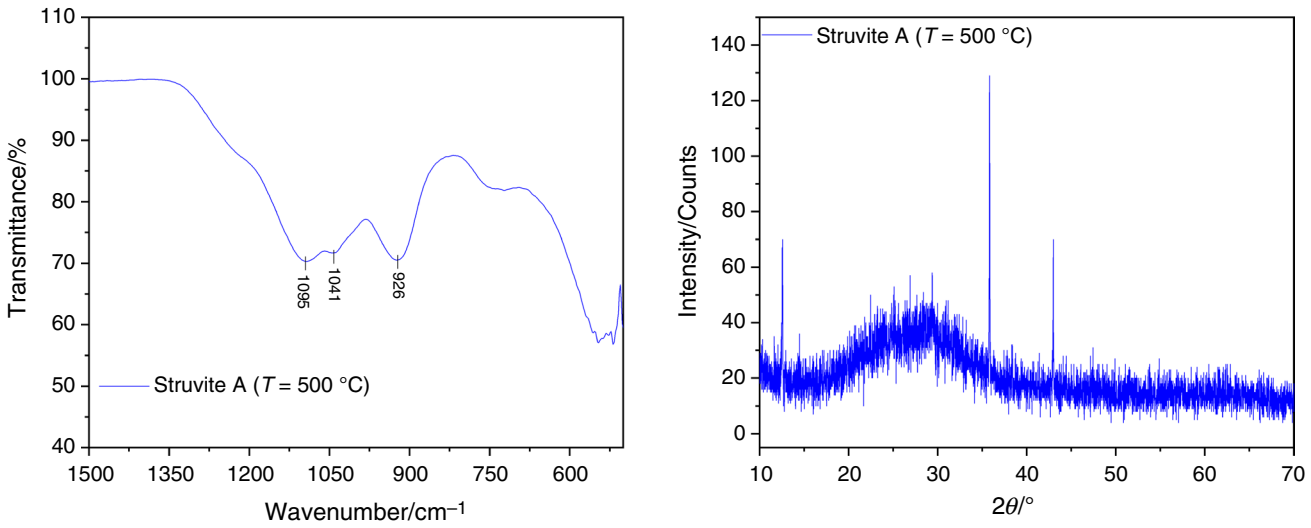


**Fig. 6** FTIR in transmittance mode (left) and XRD (right) of the calcination product of struvite A obtained from TG tests conducted up to 500 °C

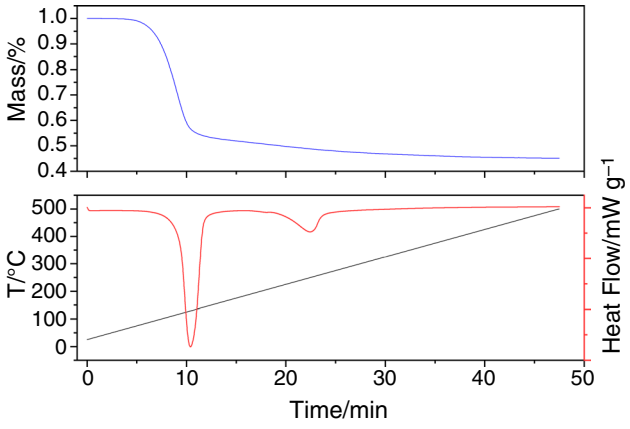


**Fig. 7** TG–DSC of struvite A at 10 °C min$^{-1}$

## Kinetic model

The kinetics of the decomposition were investigated using Friedman's isoconversional method and a model-fitting method [29, 30]. The mechanism of decomposition of struvite could be identified graphically by plotting the conversion against temperature and the derivative of the conversion with respect to temperature against the conversion of non-isothermal data (Fig. 8).

Interestingly, from the comparison of the curves with the ones reported by Khawan and Flanagan, it resulted that with $\alpha$ below 80% the curve was likely to be an order-based model or a diffusion model, but at $\alpha > 80\%$ the trend changed significantly [31]. This behaviour in the second region can also be identified as the declaratory region, where it is difficult to identify a specific kinetic model [30]. Moreover, since it is a differential method that uses exclusively experimental data, it is sensitive and graphs usually show some noise [29].

### Friedman's isoconversional method

Friedman's equation is derived by differentiating the Arrhenius equation:

$$\ln(k) = \ln A - \frac{E_a}{RT} \tag{2}$$

Since the conversion rate is expressed by:

$$\frac{d\alpha}{dt} = k(T)f(\alpha) \tag{3}$$

where $t$ is time, $\alpha$ is the conversion and $f(\alpha)$ is the reaction model, substituting Eq. 2 in Eq. 3 and rearranging it, we obtain:

$$\ln\left(\frac{d\alpha}{dt}\right)_{\alpha,i} = \ln\left(A_\alpha f(\alpha)\right) - \frac{E_{a\alpha}}{RT_i} \tag{4}$$

The index "$i$" indicates the different non-isothermal experiments conducted at different heating rates ($\beta_i$). The expression above can be rewritten as:

$$\ln\left(\beta_i \frac{d\alpha}{dT_i}\right) = \ln\left(A_\alpha f(\alpha)\right) - \frac{E_{a\alpha}}{RT_i} \tag{5}$$

At this point, by plotting $\ln\left(\beta_i \frac{d\alpha}{dT_i}\right)$ versus $1/T_i$ (K$^{-1}$) at selected values of conversion, the activation energy $E_a$ can be determined as the slope of the curve and $\ln\left(A_\alpha f(\alpha)\right)$ as the intercept. The data were plotted at intervals of conversion of 0.05.

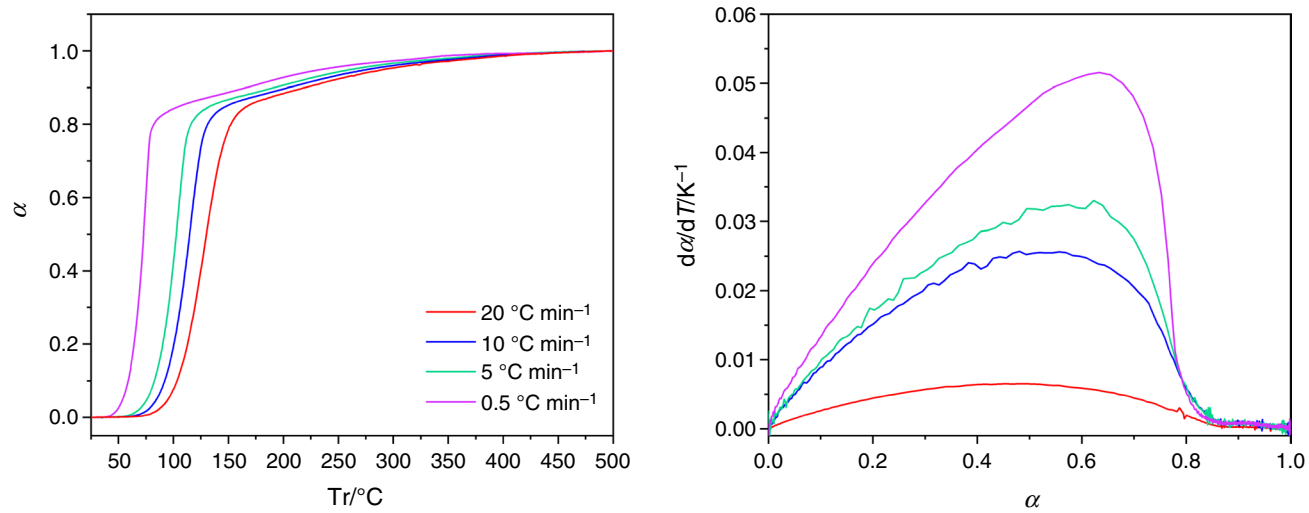


**Fig. 8** Rate of conversion $\alpha$ of struvite decomposition (left), and plot of the derivative d$\alpha$/d$T$ against conversion (right) at different heating rates

Figure 9 (left) highlights that the curves do not have the same slope. This means that the activation energy depends on conversion. In a single-stage reaction, the activation energy should be a constant value at every level of conversion. Thus, this dependency suggests that the degradation of struvite follows a multi-step process. The graphs in Fig. 9 (right), which represent both $E_a$ and $\ln\left(A_\alpha f(\alpha)\right)$ against $\alpha$, seem also to show two different behaviours: at conversions $0<\alpha<0.75$ the activation energy decreases with the temperature increase; at conversions $0.75<\alpha<1$ $E_a$ diminishes when $T$ increases (Fig. 9, right). This further proves the existence of two main reaction mechanisms occurring from heating struvite between room temperature and 500 °C. The trend equations were found with Origin software through linear regression, and all the resulted R-squared values were above 98%, confirming the good fit between the correlation and the data. Figure 9 further confirms the second region as a declaratory phase of the degradation. Therefore, the model-fitting approach will be applied only to the first step of the reaction ($0<\alpha<0.75$).

## Model-fitting method

The model-fitting approach leads to the definition of the reaction model that best fits by assuming different $f(\alpha)$ or $g(\alpha)$ and deriving the missing parameters $k(T)$ and activation energy. Although this technique is frequently used, it has a disadvantage compared to the isoconversional methods: indeed, the activation energy that results from the calculation corresponds to an average that might not detect the dependency of the variable with the conversion or temperature. To be more accurate, the best approach that identifies $E_a$ is the isoconversional method [32]. The different reaction models that express the correlation between $\alpha$ and time can be found in the literature and are shown in Table 3 [32, 33].

From the rearrangement of Eq. 3 it is possible to derive $g(\alpha)$ since it is defined as:

$$g(\alpha)=\int_0^\alpha \frac{d\alpha}{f(\alpha)}$$

Thus,

$$g_j(\alpha)=k_j(T_i)t \tag{6}$$

The following approach was applied to the data of the isothermal tests, and $g(\alpha)$ was calculated for each reaction model $j$ at different temperatures ($T_i$ = 75, 95 and 145 °C). Then, $k_j(T)$ could be derived as the slope of the curve of $g_j(\alpha)$ versus $t$. At this point, $E_{a,j}$ and $\ln A_j$ were determined at each $T_i$ using the Arrhenius equation, as done previously for the isoconversional method. Thus, the best fit could be derived using the residual sum of squares that defines the goodness of fit:

$$S_j^2=\frac{1}{n-1}\sum_{i=1}^{n}\left(\frac{t_i}{t_{0.5}}-\frac{g_j(\alpha_i)}{g_j(0.5)}\right) \tag{7}$$

In the equation above, $t_{0.5}$ is the reduced time variable that corresponds to $t/t_\alpha$ with $t_\alpha$ being the time at which the reaction has attained a specific conversion. (In this case, it has been chosen $\alpha=0.5$ as suggested in the book of solid-state kinetics by Brown et al. [34]). Once the values of $S_j^2$ are found, $F_j$ is calculated as follows:

$$F_j=\frac{S_j^2}{S^2_{\min}}$$

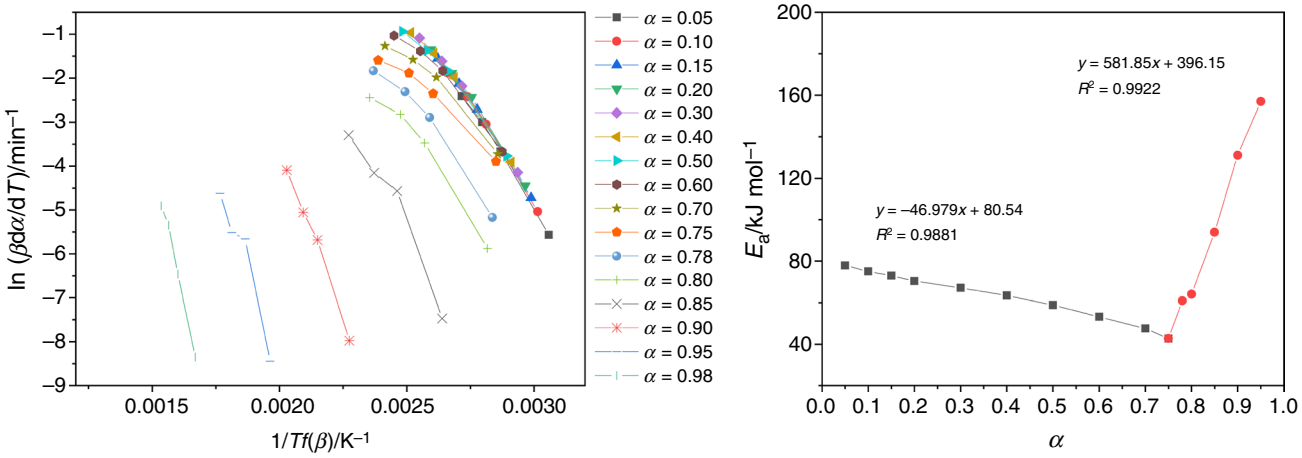


**Fig. 9** Plot of $\ln(\beta d\alpha/dT)$ versus $1/T$ of struvite for different values of $\alpha$ (left); activation energy (right) of struvite degradation derived with the Friedman's method

**Table 3** Thermal decomposition in solids expressed through reaction models

| | Reaction model | $f(\alpha)$ | $g(\alpha)$ |
|---|---|---|---|
| 1 | Power law | $4\alpha^{3/4}$ | $\alpha^{1/4}$ |
| 2 | Power law | $3\alpha^{2/3}$ | $\alpha^{1/3}$ |
| 3 | Power law | $2\alpha^{1/2}$ | $\alpha^{1/2}$ |
| 4 | Power law | $2/3\alpha^{-1/2}$ | $\alpha^{3/2}$ |
| 5 | One-dimensional diffusion | $1/2\alpha^{-1}$ | $\alpha^{2}$ |
| 6 | Mampel (first-order) | $1-\alpha$ | $-\ln(1-\alpha)$ |
| 7 | Avrami–Erofeev | $4(1-\alpha)[-\ln(1-\alpha)]^{3/4}$ | $[-\ln(1-\alpha)]^{1/4}$ |
| 8 | Avrami–Erofeev | $3(1-\alpha)[-\ln(1-\alpha)]^{2/3}$ | $[-\ln(1-\alpha)]^{1/3}$ |
| 9 | Avrami–Erofeev | $2(1-\alpha)[-\ln(1-\alpha)]^{1/2}$ | $[-\ln(1-\alpha)]^{1/2}$ |
| 10 | Three-dimensional diffusion | $2(1-\alpha)^{\frac{2}{3}}(1-(1-\alpha)^{\frac{1}{3}})^{-1}$ | $[1-(1-\alpha)^{\frac{1}{3}}]^2$ |
| 11 | Contracting sphere | $3(1-\alpha)^{2/3}$ | $1-(1-\alpha)^{1/3}$ |
| 12 | Contracting cylinder | $2(1-\alpha)^{1/2}$ | $1-(1-\alpha)^{1/2}$ |
| 13 | Second-order | $(1-\alpha)^{2}$ | $(1-\alpha)^{-1}-1$ |

**Table 4** Arrhenius parameters for struvite decomposition calculated with the model-fitting method

| Reaction model | $F=S_j^2/S_{min}^2$ | $E$/kJ mol$^{-1}$ | log($A$)/min$^{-1}$ |
|---|---|---|---|
| 1 | 7.573 | 85.97 | 23.43 |
| 2 | 7.183 | 82.71 | 22.51 |
| 3 | 6.415 | 78.30 | 21.24 |
| 4 | 2.177 | 65.21 | 17.12 |
| 5 | 1 | 60.72 | 15.59 |
| 6 | 1.148 | 61.49 | 16.72 |
| 7 | 6.651 | 80.06 | 21.88 |
| 8 | 5.945 | 76.52 | 20.91 |
| 9 | 4.552 | 71.46 | 19.53 |
| 10 | 5.583 | 52.04 | 11.46 |
| 11 | 2.112 | 64.75 | 16.40 |
| 12 | 2.645 | 66.29 | 17.17 |
| 13 | 5.243 | 50.47 | 14.08 |

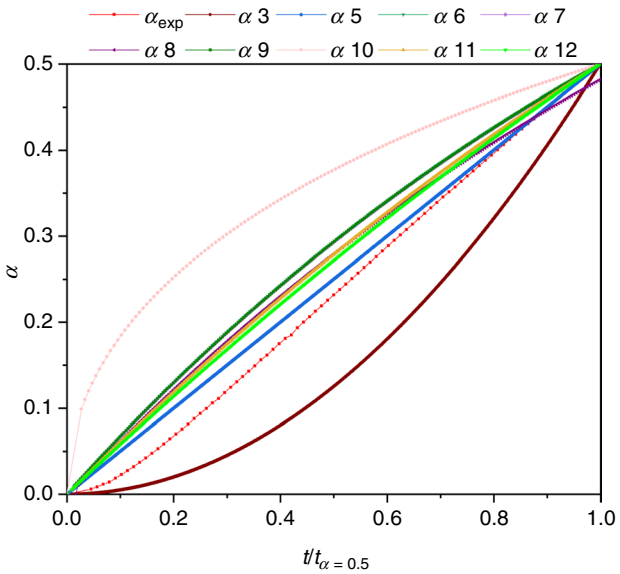


**Fig. 10** Plot of conversion of the different reaction models against reduced time at 75 °C

where $S^2_{min}$ is the smallest of $S^2_j$. The best fits could be identified as the closest to the one which presents the minimum value of the residual sum of squared.

From Table 4, it can be seen that the closest reaction models to the experimental data are models' number 5 and 6 which correspond to a one-dimension diffusion model and a first-order model. The activation energy determined for this model is 60.72 kJ mol$^{-1}$ (0.24 kJ g$^{-1}$), in accordance with the average value found for the first reaction with the Friedman's method, and comparable to the value calculated from the DSC (0.37 kJ g$^{-1}$). The conversion can be determined using Eq. 7. In order to do so, $\bar{k}_j(T)$ was calculated as the average rate constant of the three temperatures for each reaction model. Thus, for example, in case of reaction model one:

$$g_1(\alpha) = \alpha_1^{1/4} = \bar{k}(T)t$$

$$\alpha_1 = \left(\bar{k}(T)t\right)^4$$

Figure 10 reports the plot of the conversion against the reduced time at 75 °C. The experimental values of conversion marked in red resulted to have better match with the one-dimension diffusion model.

The experimental conversion is marked in red; the other curves refer to the reaction models defined in Table 2.

This suggests that the controlling factor for the first reaction occurring during the decomposition is likely to be the diffusion of ammonia and water molecules. The fact that one-dimension diffusion matched the experimental data much more closely than the three-dimensional one can be due to the fact that the data used in this analysis were gathered from the thermogravimetric experiments, which were conducted in small crucibles with small amounts of samples. Therefore, it is fair to assume that the release of ammonia and water is likely to have happened only in the vertical dimension. Thus, by combining the kinetic analysis with the thermal analysis and the characterisation analysis it can be concluded that the first reaction transformed struvite into $MgHPO_4$ (Eq. 8), as can be confirmed by the FTIR spectra, even though not all ammonia is removed.

$$MgNH_4PO_4 \cdot 6H_2O_{(s)} \rightarrow MgHPO_{4(s)} + NH_{3(g)} \uparrow + 6H_2O_{(g)} \uparrow \quad (8)$$

The reaction is regulated by diffusion of water and ammonia molecules from the solid to the gas phase. From 250 to 500 °C, the decomposition undergoes a second step, as also highlighted in the DSC experiment, from which $MgHPO_4$ is transformed into $Mg_2P_2O_7$ (Eq. 9).

$$2MgHPO_{4(g)} \rightarrow + Mg_2P_2O_{7(s)} + H_2O_{(g)} \uparrow \quad (9)$$

## Conclusions

Struvite decomposition in the solid state was investigated to understand whether ammonia could be released and recovered as a more valuable product, and the magnesium source could be recycled in the system, saving part of the costs of the expensive chemical used. Thermogravimetric analysis showed the influence of the heating rate in the decomposition of struvite: the calcination onset temperature decreased at lower heating rates, confirming results from previous studies. At 0.5 °C $min^{-1}$, the decomposition started at circa 31 °C. However, ammonia could not be completely released below 250 °C, as shown from the infrared spectra. The final calcination product was found to be magnesium pyrophosphate. Although thermogravimetric analysis and the first derivative displayed one main peak, the differential scanning calorimetry technique highlighted the presence of two major events that represent a change in the phase or in the structure of the sample. This result was also confirmed by the kinetic analysis that revealed the presence of two different reactions. The kinetic analysis highlighted that the first one (which is from conversion equal to zero to conversion equal to 0.75) is likely to be an order-based or diffusion model, meaning that diffusion is the main phenomenon controlling the decomposition. The energy required to complete the degradation, calculated from the DSC curves, was found to be 1.87 kJ $g^{-1}$ at 10 °C $min^{-1}$. These findings provided new insights regarding the thermal decomposition of struvite, since understanding the kinetic mechanism and the energy required will help in the optimisation of the design of the recovery technology.

**Acknowledgements** Funding was provided by EPSRC (Grant No. EP/L016389/1) and Severn Trent Water PLC.



## References

1. Peccia J, Westerhoff P. We should expect more out of our sewage sludge. Environ Sci Technol. 2015;49:8271–6. https://doi.org/10.1021/acs.est.5b01931.
2. Ellen Macarthur Foundation, Circular Economy Overview, Ellen MacArthur Found. https://www.ellenmacarthurfoundation.org/circular-economy/overview/concept (2017). Accessed June 25, 2018.
3. Dawson CJ, Hilton J. Fertiliser availability in a resource-limited world: production and recycling of nitrogen and phosphorus. Food Policy. 2011;36:973–9. https://doi.org/10.1016/j.foodpol.2010.11.012.
4. USGS, Nitrogen (fixed)–Ammonia. https://minerals.usgs.gov/minerals/pubs/commodity/nitrogen/mcs-2018-nitro.pdf (2018). Accessed August 7, 2018.
5. Smil V. Detonator of the population explosion. Nature. 1999;400:415.
6. Ashik UPM, Wan Daud WMA, Abbas HF. Production of greenhouse gas free hydrogen by thermocatalytic decomposition of methane: A review. Renew. Sustain. Energy Rev. 2015;44:221–56. https://doi.org/10.1016/j.rser.2014.12.025.
7. Fraile D, Lanoix J-C, Maio P, Rangel A, Torres A. Overview of the market segmentation for hydrogen across potential customer groups based on key application areas. 2015. https://www.certifhy.eu/images/D1.1_Bibliographic_review_of_market_outlooks_for_hydrogen_in_Europe.pdf. Accessed 7 Aug 2018.
8. Zarebska A, Romero Nieto D, Christensen KV, Fjerbæk Søtoft L, Norddahl B, Nieto DR, Christensen KV, Sotoft LF, Norddahl B. Ammonium fertilizers production from manure: a critical review. Crit. Rev. Environ. Sci. Technol. 2014;45:1469–521. https://doi.org/10.1080/10643389.2014.955630.
9. Romero-Güiza MS, Tait S, Astals S, del Valle-Zermeño R, Martínez M, Mata-Alvarez J, Chimenos JM. Reagent use efficiency with removal of nitrogen from pig slurry via struvite: a study on magnesium oxide and related by-products. Water Res. 2015;84:286–94. https://doi.org/10.1016/j.watres.2015.07.043.
10. Doyle JD, Parsons SA. Struvite formation, control and recovery. Water Res. 2002;36:3925–40. https://doi.org/10.1016/S0043-1354(02)00126-4.
11. Borgerding J. Phosphate deposits in digestion systems. J. Wastewater Pollut. Control Fed. 1972;44:813–9.
12. Bhuiyan RDBMIH, Mavinic DS. A solubility and thermodynamic study of struvite. Environ. Technol. 2007;28:1015–26. https://doi.org/10.1080/09593332808618857.

13. Frost RL, Weier ML, Erickson KL. Thermal decomposition of struvite. J. Therm. Anal. Calorim. 2004;76:1025–33. https://doi.org/10.1023/B:JTAN.0000032287.08535.b3.
14. Bhuiyan MIH, Mavinic DS, Koch FA. Thermal decomposition of struvite and its phase transition. Chemosphere. 2008;70:1347–56. https://doi.org/10.1016/j.chemosphere.2007.09.056.
15. Chen Y, Tang J, Li W, Zhong Z, Yin J. Thermal decomposition of magnesium ammonium phosphate and adsorption properties of its pyrolysis products toward ammonia nitrogen. Trans. Nonferrous Met. Soc. China. 2015;25:497–503. https://doi.org/10.1016/S1003-6326(15)63630-5.
16. Sugiyama S, Yokoyama M, Ishizuka H, Sotowa K-I, Tomida T, Shigemoto N. Removal of aqueous ammonium with magnesium phosphates obtained from the ammonium-elimination of magnesium ammonium phosphate. J. Colloid Interface Sci. 2005;292:133–8. https://doi.org/10.1016/j.jcis.2005.05.073.
17. Kumar R, Pal P. Turning hazardous waste into value-added products: production and characterization of struvite from ammoniacal waste with new approaches. J. Clean. Prod. 2013;43:59–70. https://doi.org/10.1016/j.jclepro.2013.01.001.
18. He S, Zhang Y, Yang M, Du W, Harada H. Repeated use of MAP decomposition residues for the removal of high ammonium concentration from landfill leachate. Chemosphere. 2007;66:2233–8. https://doi.org/10.1016/j.chemosphere.2006.09.016.
19. Zhang T, Li P, Fang C, Jiang R. Phosphate recovery from animal manure wastewater by struvite crystallization and $CO_2$ degasification reactor. Ecol. Chem. Eng. S. 2014;21:89–99. https://doi.org/10.2478/eces-2014-0008.
20. Le Corre KS, Valsami-Jones E, Hobbs P, Parsons SA. Impact of calcium on struvite crystal size, shape and purity. J. Cryst. Growth. 2005;283:514–22. https://doi.org/10.1016/j.jcrysgro.2005.06.012.
21. Zhang T, Ding L, Ren H. Pretreatment of ammonium removal from landfill leachate by chemical precipitation. J. Hazard Mater. 2009;166:911–5. https://doi.org/10.1016/j.jhazmat.2008.11.101.
22. Matynia A, Wierzbowska B, Hutnik N, Mazienczuk A, Kozik A, Piotrowski K. Separation of struvite from mineral fertilizer industry wastewater. Procedia Environ. Sci. 2013;18:766–75. https://doi.org/10.1016/j.proenv.2013.04.103.
23. Ali MI. Struvite crystallization in fed-batch pilot scale and description of solution chemistry of struvite. Chem. Eng. Res. Des. 2007;85:344–56. https://doi.org/10.1205/cherd06031.
24. Ostara Nutrient Recovery Technologies Inc., Turn Problematic Struvite Into Premium, High Value, Market-Ready Fertiliser, 2018. http://ostara.com/wp-content/uploads/2018/04/EU_Ostara_Crystal-Green_Handout.pdf.
25. European Commission, Regulation (EC) No 2003/2003 of the European Parliament and of the Council of 13 October 2003 relating to fertilisers, 2003.
26. Yu R, Ren H, Wang Y, Ding L, Geng J, Xu K, Zhang Y. A kinetic study of struvite precipitation recycling technology with NaOH/$Mg(OH)_2$ addition. Bioresour. Technol. 2013;143:519–24. https://doi.org/10.1016/j.biortech.2013.06.042.
27. Ramlogan MV, Rouff AA. An investigation of the thermal behavior of magnesium ammonium phosphate hexahydrate. J. Therm. Anal. Calorim. 2016;123:145–52. https://doi.org/10.1007/s10973-015-4860-1.
28. Boonchom B. Kinetic and thermodynamic studies of $MgHPO_4 \cdot 3H_2O$ by non-isothermal decomposition data. J. Therm. Anal. Calorim. 2009;98:863. https://doi.org/10.1007/s10973-009-0108-2.
29. Šimon P. Isoconversional methods: fundamentals, meaning and application. J. Therm. Anal. Calorim. 2004;76:123–32. https://doi.org/10.1023/B:JTAN.0000027811.80036.6c.
30. Bamford CH, Tipper CFH. Theory of solid state reaction kinetics. In: Bamford CH, Tipper CFH, editors. Comprehensive chemical kinetics, vol. 22, reaction in the solid state. Amsterdam: Elsevier; 1980. p. 41–113.
31. Khawan A, Flanagan RD. Solid-state kinetic models: basic and mathematical fundamentals. J. Phys. Chem. B. 2006;110:17315–28. https://doi.org/10.1021/jp062746a.
32. Vyazovkin S, Wight CA. Model-free and model-fitting approaches to kinetic analysis of isothermal and nonisothermal data. Thermochim. Acta. 1999;340–341:53–68. https://doi.org/10.1016/S0040-6031(99)00253-1.
33. Burnham AK. Introduction to chemical kinetics. In: Global chemical kinetics of fossil fuels how to model maturation and pyrolysis, 2017. p. 25–74. https://doi.org/10.1007/978-3-319-49634-4.
34. Brown ME, Dollimore D, Galwey A. Reactions in the solid state. Compr. Chem. Kinet. 1980. https://doi.org/10.1016/S0167-6881(99)80004-4.